Facile Fabrication of Hierarchical MOF-Metal Nanoparticle Tandem Catalysts for the Synthesis of Bioactive Molecules

Jingwen Chen,[†,‡] Biying Zhang,[‡] Long Qi,[§] Yuchen Pei,[‡] Renfeng Nie,[‡] Patrick Heintz,[‡] Xuechen Luan,[‡] Zongbi Bao,[†] Qiwei Yang,[†] Qilong Ren,[†] Zhiguo Zhang,*[,†] and Wenyu Huang*[,‡,§]

[†]Key Laboratory of Biomass Chemical Engineering of Ministry of Education, College of Chemical and Biological Engineering, Zhejiang University, Hangzhou 310027, China

[‡]Department of Chemistry, Iowa State University, Ames, IA 50011, USA

[§]Ames Laboratory, U.S. Department of Energy, Ames, IA 50011, USA

KEYWORDS

tandem reaction, metal-organic frameworks, hierarchical pore, heterogeneous catalysis, bioactivity, quinoline *N*-oxides

ABSTRACT

Multifunctional metal-organic frameworks (MOFs) that possess permanent porosity are promising catalysts in organic transformation. Herein, we report the construction of a hierarchical MOF functionalized with basic aliphatic amine groups and polyvinylpyrrolidone-capped platinum nanoparticles (Pt NPs). The post-synthetic covalent modification of organic ligands increases basic site density in the MOF, and simultaneously introduce mesopores to create a hierarchically porous structure. The multifunctional MOF is capable of catalyzing a sequential Knoevenagel condensation–hydrogenation–intramolecular cyclization reaction. The unique selective reduction of nitro group to intermediate hydroxylamine by Pt NPs supported on MOF, followed by intramolecular cyclization with cyano group to afford an excellent yield (up to 92%) to the uncommon quinoline *N*-oxides over quinolines. The hierarchical MOF and polyvinylpyrrolidone capping agent on Pt NPs synergistically facilitate the enrichment of substrates, and thus lead to high activity in the reduction–intramolecular cyclization reaction. The bioactivity assay indicates that the synthesized quinoline *N*-oxides evidently inhibit the proliferation of lung cancer cells. Our findings demonstrated the feasibility of MOF-catalyzed direct synthesis of bioactive molecules from readily available compounds under mild conditions.

Introduction

The increasingly severe concerns on growing energy consumption, depleting natural resources, and increasing pollutant emission prompt us to find energy- and atom- efficient processes for chemical production. One of the effective strategies is to synthesize organic compounds via tandem reactions,[1,2] which can avoid the separation and purification of reaction intermediates, minimize the waste generation and energy input, and greatly facilitate process intensification.[3,4] To realize a tandem reaction, efficient multifunctional catalysts are required that can catalyze all individual reaction steps involved.[5]

Multifunctional heterogeneous catalysts, which can integrate different types of active sites within one solid material, have attracted considerable research attention in tandem catalysis. Metal-organic frameworks (MOFs),[6] constructed by the coordination of metal ions or clusters with organic linkers, are promising materials as tandem catalysts because of their intrinsic structure properties.[7-12] The pore size, topology, and chemical functionality of MOFs can be fine-tuned by varying the metal ions or organic ligands.[13-15] Additionally, other active sites like metal NPs can be easily introduced on or into MOF.[16-19] However, most of the reported MOFs are microporous, which hinders the mass transfer and decrease the accessibility of active sites inside MOFs. In this context, the construction of multifunctional MOFs with hierarchical porous structure[20] for tandem reaction is worthy of in-depth investigations.

In line with the growing interest of the multifunctional MOFs in the synthesis of bioactive molecules,[21] we focused on the synthesis of quinoline *N*-oxides, as representative *N*-containing heterocycles that widely exist in natural products known for biological activity[22] in anti-cancer,[23] antibacterial,[24] antimalarial,[25] and antifungal[26] applications. Quinoline *N*-oxides can also serve as

organocatalysts[27] or ligands for metal complexes with catalytic activity[28] and optical and magnetic functions.[29,30] Moreover, quinoline *N*-oxides are vital precursors[31,32] for the synthesis of various quinoline derivatives, which cannot be easily accessed from quinoline due to its low activity and poor regioselectivity.[33-36]

Despite the above mentioned superior properties and vast applications, the synthesis of quinoline *N*-oxides is considerably underdeveloped. Previously reported methods for the synthesis of quinoline *N*-oxides include the oxidation of quinolines,[37,38] reductive cyclization reaction of 2-nitrochalcones,[39] and others.[40,41] However, both quinolines and 2-nitrochalcones are not readliy available.[40,42] Moreover, most of the reported methods encountered with chanllenges, such as harsh reaction conditions,[43] poor selectivity,[44] and tedious separation procedures. Hence, for the synthesis of quinoline *N*-oxides, it is highly advantageous to develop a tandem catalytic system that can obtain *o*-nitroaryl compounds *in situ* from simple and affordable starting materials under mild conditions, and the key is the design and construction of multifunctional tandem catalysts.

Herein, we reported a multifunctional tandem MOF-based catalyst for the synthesis of quinoline *N*-oxides from readily available *o*-nitrobenzaldehydes and malononitrile via a one-pot tandem Knoevenagel condensation–hydrogenation–intramolecular cyclization reaction. A convenient post-synthetic modification method[45,46] was developed to simultaneously increase the basic site density and create a hierarchically porous structure of a Zr-MOF. Polyvinylpyrrolidone (PVP)-capped Pt NPs were supported on the Zr-MOF to construct the tandem catalyst. A bioactivity assay shows that the obtained quinoline *N*-oxides can inhibit the growth of lung cancer cells, HepG2, in a dose-dependent manner. This work demonstrates the development of a MOF-based multifunctional catalyst and a new tandem catalytic strategy for the preparation of chemicals with potential anti-cancer activities.

Results and Discussion

Synthesis and Characterization

UiO-66-NH_2 is assembled from $ZrCl_4$ and 2-aminoterephthalic acid ligand under hydrothermal reaction conditions,[47,48] which possesses uniform cavities and exceptional stability. Powder X-ray diffraction (PXRD) pattern of the as-synthesized UiO-66-NH_2 is identical with the simulated pattern of UiO-66-NH_2 (Figure 1A).[49] The basic site density of MOF was increased by introducing aliphatic amine group via post-synthetic modification (PSM) of UiO-66-NH_2 according to a method modified from literature.[46] The amine tags on the ligand (2-aminoterephthalic acid, BDC-NH_2) of UiO-66-NH_2 was alkylated with 2-dimethylaminoethyl chloride hydrochloride (see Supporting Information), the resulted material was denoted as UiO-NM. The new pendent aliphatic amine has thus been introduced into MOF pores, which was anticipated to enhance the basicity of UiO-66-NH_2. As illustrated by the PXRD patterns (Figure 1A), the crystallinity of the MOF maintains after the PSM. ^{1}H NMR spectrum of the digested sample of UiO-NM (Figure S1) shows that the molar ratio of the BDC-NH_2 and its *N*,*N*-dimethylaminoethyl modified form is 2.3:1.0, implying that ~30% BDC-NH_2 linkers of the MOF are modified.

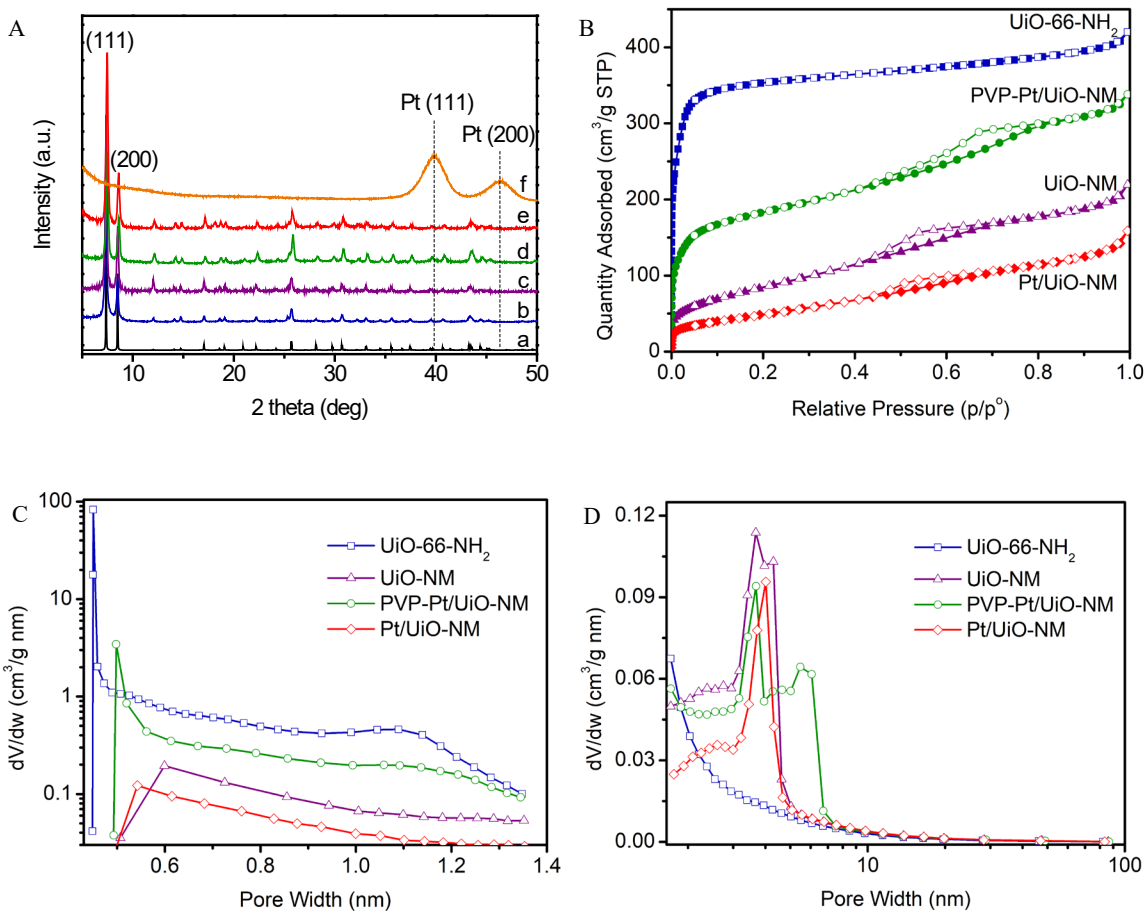

Figure 1. (A) PXRD patterns of (a) simulated UiO-66-NH_2, (b) UiO-66-NH_2, (c) UiO-NM, (d) PVP-Pt/UiO-NM, (e) Pt/UiO-NM and (f) PVP-Pt NPs. (B) N_2 physisorption isotherms and (C, D) pore size distribution of UiO-66-NH_2, UiO-NM, PVP-Pt/UiO-NM, and Pt/UiO-NM measured at 77 K. Filled and open circles in (B) represent adsorption and desorption branches, respectively.

A decrease in Brunauer–Emmett–Teller (BET) surface area and pore volume (Figure 1B, Table S1) was observed due to the introduction of alkyl amine group. Surprisingly, 2-5 nm mesopores were formed in UiO-NM (Figure 1D), possibly due to the partial etching of UiO-66-NH_2 during the PSM.[50-52] These mesopores add an additional benefit to the catalysts, facilitating the diffusion of molecules inside the pores and thus improving the efficiency of the catalyst. After confirming the successful introduction of aliphatic amine groups, PVP-Pt NPs were loaded on UiO-NM (PVP-

Pt/UiO-NM). Surprisingly, we found PVP-Pt/UiO-NM has a significantly increased surface area and pore volume in comparison to UiO-NM. The pore size distribution plot in Figure 1D clearly shows that loading PVP-Pt NPs on UiO-NM creates additional 5-7 nm mesopores, possibly due to the PVP-induced stacking of MOF particles and the sonication of the sample during the loading of PVP-Pt NPs onto UiO-NM. However, loading PVP-Pt NPs onto UiO-66-NH_2, following exactly the same method, does not create 5-7 nm mesopores (Figure S2). We could not find any literature that reports the formation of mesopores by loading NPs onto microporous MOFs, which needs more studies to fully understand the exact mechanism. The increase in the surface area and pore volume of PVP-Pt/UiO-NM also indirectly suggested that the PVP-Pt NPs are located on the external surface of the MOF. Otherwise, there should be an apparent decrease in N_2 adsorption due to the occupation of the MOF pores by PVP-Pt NPs. We further confirmed this by preparing PVP-free Pt NPs supported in the MOF (Pt/UiO-NM) by impregnation method (see Supporting Information), where majority Pt NPs will form in the internal pores of the MOF due to the strong Pt-NH_2 interaction.[53] As expected, the PVP-free Pt/UiO-NM showed a dramatically decreased surface area and pore volume (Figure 1B, Table S1). The XRD patterns of Pt/UiO-NM (Figure 1A) indicated that the crystallinity of MOF was well retained after loading the metal precursor and subsequent reduction process.

Transmission electron microscopy (TEM) indicated that PVP-capped Pt NPs were mainly dispersed on the external surface of UiO-NM uniformly (Figure 2),[53,54] the mean diameter of PVP-Pt NPs is 2.9 nm. Additional tilting experiments revealed the protruding of NPs from the edge of the MOF while we rotated the sample in TEM, which further confirmed that PVP-Pt NPs are located on the external surface of the MOF (Figure S3). A high-resolution TEM (HRTEM) image (Figure 2C) showed that one of those dark particles has a lattice spacing of 0.23 nm, corresponding

to the [111] plane of Pt. At the same Pt loading as PVP-Pt/UiO-NM, Pt/UiO-NM prepared by the impregnation method shows a significantly low density of Pt NPs on the surface of the MOF (Figure S4), indicating the majority of Pt NPs are confined inside the internal pores of the MOF.

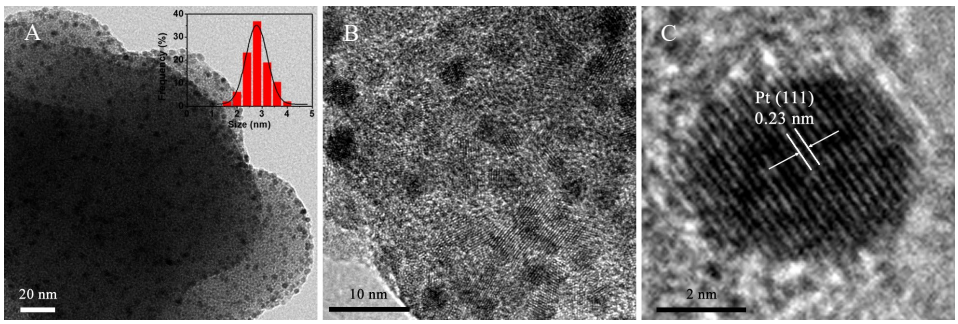

Figure 2. (A) TEM images and Pt NPs size distribution of PVP-Pt/UiO-NM. (B, C) HRTEM images of PVP-Pt NPs supported on UiO-NM. Pt loading is 1.6 wt% determined by inductively coupled plasma mass spectroscopy (ICP-MS).

X-ray photoelectron spectroscopy (XPS) was performed to investigate the surface property and chemical state of PVP-Pt/UiO-NM (Figure S5). The binding energies (BE) are referenced to the C1s peak position at 284.6 eV. Two main peaks centered at 70.8 and 74.1 eV can be ascribed to the Pt $4f_{7/2}$ and Pt $4f_{5/2}$, respectively. These two peaks can be deconvoluted into two pairs of peaks, which correspond to metallic Pt (70.8 and 74.1 eV), Pt^{2+} (72.1 and 75.4 eV), respectively. The metallic Pt (86 at.%) is the predominant species.

Tandem Reaction for the Synthesis of Quinoline *N*-Oxide

After synthesis and characterization, we investigated the activity of PVP-Pt/UiO-NM in catalyzing the tandem Knoevenagel condensation–reduction–cyclization reaction. The catalytic

properties of the catalysts on the Knoevenagel condensation reaction between 2-nitrobenzaldehyde and malononitrile was evaluated at first (Figure S6). The reaction rate was enhanced obviously when the condensation was catalyzed by PVP-Pt/UiO-NM as compared with that by PVP-Pt/UiO-66-NH_2. The acceleration effect can be attributed to the introduction of the mesopores and the increased basic site density of MOF after the PSM process based on the initial reaction rate determined while the conversion is below 20% (Table S4). The PVP-free Pt/UiO-NM control catalyst shows a much inferior catalytic activity than PVP-Pt/UiO-NM, which could be caused by the lower BET surface area (Table S1) and the partial blockage of the MOF pores by Pt NPs. We also noticed that the loading of PVP-Pt onto MOFs slows down the Knoevenagel condensation reaction. The loaded PVP-Pt NPs on UiO-NM, even located primarily on the surface of UiO-NM, could still partially block the opening of the pores and hinder reactants from accessing the internal basic sites of MOFs for the condensation reaction.

We then explored the reaction between 2-nitrobenzaldehyde and malononitrile catalyzed by PVP-Pt/UiO-NM under hydrogen atmosphere (one-pot and one-step), in anticipation to obtain quinoline *N*-oxide **4a** by a one-pot tandem reaction. Quinoline *N*-oxide **4a** was formed in 47% yield (Table S5, entry 1) in accompany with the hydrogenation product of 2-nitrobenzaldehyde and a small amount of quinoline **5a**. When replacing Pt with an equivalent molar amount of Pd (Table S5, entry 2), both the yield of **4a** and the selectivity of **4a** over **5a** decreased. Therefore, Pt was chosen for further studies. We also observed that increasing the reaction temperature from 60 to 80°C did not improve the yield of quinoline *N*-oxide but a decreased temperature can improve the selectivity of *N*-oxide over quinoline (**4a**:**5a** ratio in Table S5, entries 3-5).

In order to increase the selectivity and yield to quinoline *N*-oxide, we then tried the tandem reaction in one-pot but two sequential steps: i) base-catalyzed Knoevenagel condensation; ii)

platinum-catalyzed hydrogenation of nitro group and subsequent intramolecular cyclization reaction. At first, the reaction conditions for the Knoevenagel condensation reaction was fixed at 100°C for 5 h to ensure full conversion of 2-nitrobenzaldehyde. After the condensation step, the mixture was subjected to hydrogenation reaction without any purification. The catalytic hydrogenation was conducted over PVP-Pt/UiO-NM and Pt/UiO-NM at 80°C for 18 h. PVP-Pt/UiO-NM gave 62% yield of quinoline *N*-oxide **4a** (Table 1, entry 2), while Pt/UiO-NM showed inferior activity toward the hydrogenation reaction (Table 1, entry 1). By decreasing the temperature from 80°C to 23°C (Table 1, entries 2-4), the yield of quinoline *N*-oxide can be improved significantly. We also found that the hydrogenation reaction can proceed smoothly under lower hydrogen pressure (Table 1, entries 4-6). The best result was obtained at 23°C under 1 atm of hydrogen (Table 1, entry 6). The mild synthetic conditions make it attractive for industrial application.

Table 1. Optimization of the Reaction Conditions in the Reductive Cyclization Reaction[a]

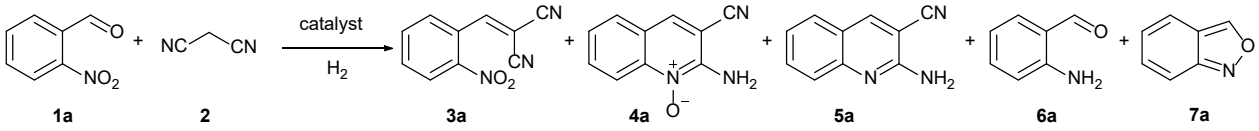

entry	catalyst	T (°C)	H_2 (psi)	yield (%)[b]			**4a**:**5a** (%)[c]
				4a	**5a**	others	
1	Pt/UiO-NM	80	400	5	2	94	2.5:1
2	PVP-Pt/UiO-NM	80	400	62	8	30	7.8:1
3	PVP-Pt/UiO-NM	60	400	75	4	21	18.8:1
4	PVP-Pt/UiO-NM	23	400	88	2	10	44:1
5	PVP-Pt/UiO-NM	23	200	84	2	14	42:1

6	PVP-Pt/UiO-NM	23	14.7	92	<1	7	>92:1

[a] Reaction conditions: step 1) 2-nitrobenzaldehyde (0.1 mmol), malononitrile (2 equiv.), catalyst (10 mg, 0.8 mol% Pt), toluene (1 mL), 100 °C, and 5 h; step 2) hydrogenation under the conditions showed in the table for 18 h. [b] Determined by ^{1}H NMR with mesitylene as the internal standard. [c] Molar ratio of **4a**:**5a** determined by ^{1}H NMR by integrating the characteristic peaks.

We found a synergistic effect between PVP-Pt and the MOF in the reductive cyclization reaction of **3a**. PVP-Pt NPs are highly dispersed by UiO-NM, whose surface active sites are more accessible by the substrate. On the contrary, PVP-Pt without the MOF support gave only 5% of **4a** in the reductive cyclization reaction of **3a** (Table S7, entry 2). Clearly, MOF support can prevent PVP-Pt NPs from aggregation and lead to more efficient hydrogenation of the nitro group.

The superior catalytic activity of PVP-Pt/UiO-NM encouraged us to further investigate the role of PVP and MOF support. UV-vis spectroscopy was used to investigate the adsorption of the substrate **3a** on different solids (Figures S7 and S8). To a solution of **3a** was added different catalysts, and the concentration of **3a** in the supernatant was monitored by UV-vis. The amount of **3a** adsorbed at the first 0.5 h was displayed in Figure 3A. UiO-NM adsorbed ~9.5 mg of **3a**, and an even higher adsorption amount was observed for PVP-Pt/UiO-NM, which agrees with the increase of surface area and pore volume after loading PVP-Pt NPs (Table S1). On the contrary, Pt/UiO-NM only adsorbed small amount of **3a,** due to the low surface area and the blockage of the MOF internal pores by Pt NPs. As illustrated in Figure 3B, the adsorption rate of **3a** by PVP-Pt/UiO-NM is also higher than the control catalysts and the support. Therefore, the combination of UiO-NM and PVP on Pt NPs promotes the substrate adsorption synergistically, which

contributes to the enhanced catalytic activity of PVP-Pt/UiO-NM toward the reductive cyclization reaction.[55]

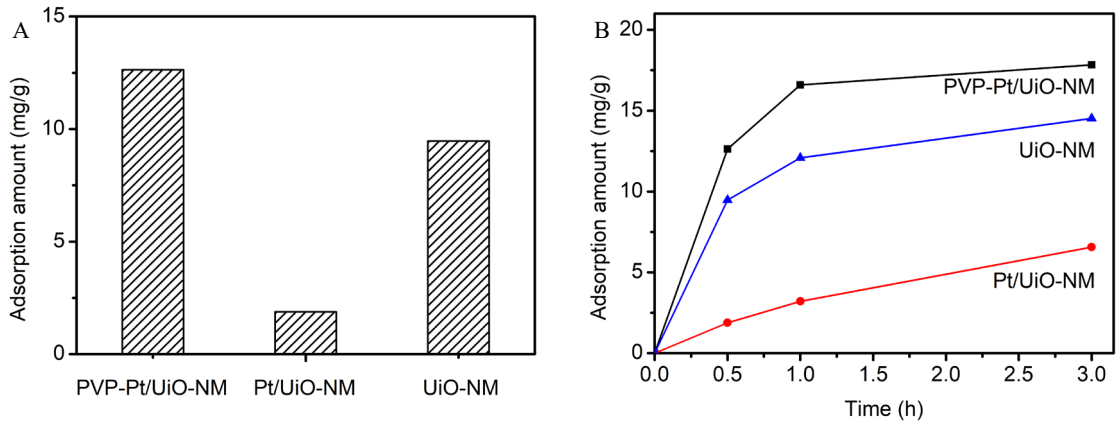

Figure 3. (A) Adsorption amount of **3a** with different solid at an adsorption time of 0.5 h. (B) Adsorption amount of **3a** with (a) PVP-Pt/UiO-NM, (b) UiO-NM and (c) Pt/UiO-NM at different adsorption time.

Next, the influence of solvent and catalyst loading on the reductive cyclization reaction was investigated (Figure S9). The polar protonic solvent and non-protonic solvents resulted in inferior yield and selectivity toward quinoline *N*-oxide **4a** (Figure S9A). The non-polar toluene is the best solvent for the selective synthesis of quinoline *N*-oxide. A catalyst loading lower than 10 mg (Figure S9B) will decrease the yield, but the selectivity of **4a** against **5a** maintained. Further increment of the catalyst amount can't improve the yield. We also optimized the reaction temperature for the Knoevenagel condensation reaction and found 80°C is enough to achieve the full conversion within 5 h (Figure S10). Hence, the optimized reaction conditions for the tandem reaction is 80°C for 5 h in the Knoevenagel condensation, and 1 bar of H_2 at 23°C for 18 h in the reductive cyclization.

With the optimized reaction conditions in hand, we then applied this protocol to other 2-nitrobenzaldehydes (Table 2). The electro-withdrawing substituents (Table 2, entries 2-4) has a minor influence on the reaction rate or product yield. While with the electron-donating group (Table 2, entry 5), the *N*-oxide was formed in moderate yield. Few examples of heterogeneously catalyzed synthesis of quinoline *N*-oxides have been reported so far. Namboothiri et al. employed carbon nanotube–ruthenium hybrids as catalyst.[39] However, the yield of quinoline *N*-oxides (trace to 79%) was not satisfactory and complex starting materials and large excess amount of reducing agents are required. Other MOFs supported metal NPs yield quinolines as the major products,[21,56] which demonstrated the unique composition and pore structure of PVP-Pt/UiO-NM for the selective synthesis of quinoline *N*-oxides.

Table 2. Substrate Scope of the Tandem Reaction[a]

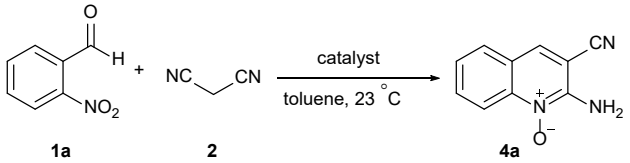

1a 2 4a

entry	product	yield (%)[b]
1	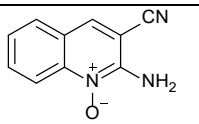 4a	81
2	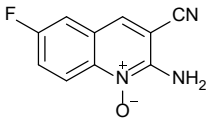 4b	82
3	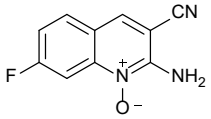 4c	84
4	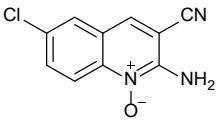 4d	78

5	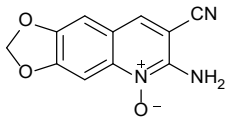 **4e**	58

[a] Reaction conditions: step 1) **1** (0.1 mmol), malononitrile (2 equiv.), PVP-Pt/UiO-NM (10 mg, 0.8 mol% Pt), toluene (1 mL) was stirred at 80°C for 5 h. Step 2) hydrogenated at 23 °C under 1 bar of H_2 for 18 h. [b] Yield of isolated product.

To evaluate the stability and recyclability of the catalyst, the reaction was conducted with the recovered catalyst for several runs. The catalytic activity and selectivity of PVP-Pt/UiO-NM retained after 3 consecutive runs and we can achieve ~90% product yield of **4a** (Table S8) under the standard reaction conditions. To further probe into the stability of the catalyst, both Knoevenagel condensation and reductive cyclization recycle reactions at a low conversion level were investigated separately. For the Knoevenagel condensation step, the conversion of 2-nitrobenzaldehyde decreased during the first three runs and maintained from the 3rd to the 5th runs (Figure S11). For the reductive cyclization step, the yield of quinoline *N*-oxide **4a** was maintained after six consecutive runs (Figure S12). The PXRD patterns (Figure S13) and N_2 sorption isotherm (Figure S14 and Table S9) indicated that the crystallinity and pore structure of used PVP-Pt/UiO-NM were largely maintained, which demonstrated the reusibility of UiO-NM under the reaction conditions. PVP-Pt NPs dispersed uniformly after five consecutive runs and the particle size remains the same without any obvious aggregation (Figure S15). These results further verify the stability of the catalyst under the tandem reaction conditions. A filtration test was also conducted to see if any catalytic species leached into the reaction mixture. The catalyst was removed from the reaction mixture by centrifugation after hydrogenating for 2 h. The supernatant was divided

into two equal portions, one portion was analyzed by ^{1}H NMR, another portion was stirred continuously under hydrogen for another 16 h. No further conversion of **3a** was observed (Table S10), which confirms the heterogeneity of the catalyst.

Based on the experimental results, a plausible reaction mechanism was proposed (Scheme 1). Under the catalysis of basic sites of UiO-NM, 2-nitrobenzaldehyde and malononitrile were condensed to form the Knoevenagel condensation product **3a**. Then, nitro group was selectively reduced to hydroxylamine **8** and underwent the intramolecular cyclization reaction with cyano group,[39,57] which affords the quinoline *N*-oxides **4a**. Unlike most of the work reported before, further hydrogenation of hydroxylamine to amine **9** was prevented in this catalytic system, hence a high selectivity of quinoline *N*-oxide over quinoline was obtained.

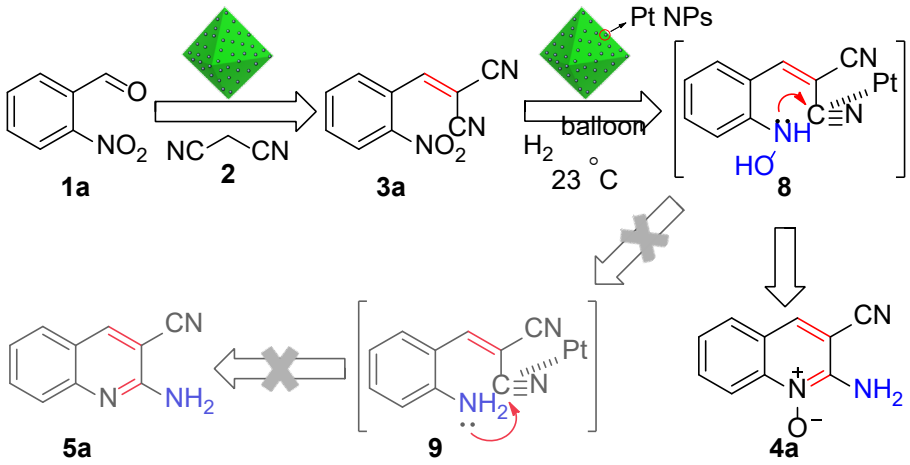

Scheme 1. Plausible Reaction Mechanism of PVP-Pt/UiO-NM Catalyzed Synthesis of Quinoline *N*-Oxide.

Bioactivity of Quinoline *N*-Oxide

Quinoline *N*-oxides has attracted great research interests due to its potential pharmacological activities. After obtaining different quinoline *N*-oxide structures, we then investigated whether it can affect the proliferation of lung cancer cells, HepG2. To see the effect, we cultured the HepG2 cell in the presence of quinoline *N*-oxides at different concentrations. As showed in Figure 4, quinoline *N*-oxides reduced the growth of HepG2 cells, and the inhibition effect is depended on the compound concentration. As compared with the untreated cells, an obvious decrease in the cell viability was observed with 90 μM quinoline *N*-oxide **4e** (⩾53%). The results suggested that quinoline *N*-oxide structure has promising bioactivity for inhibiting cancer cell growth.

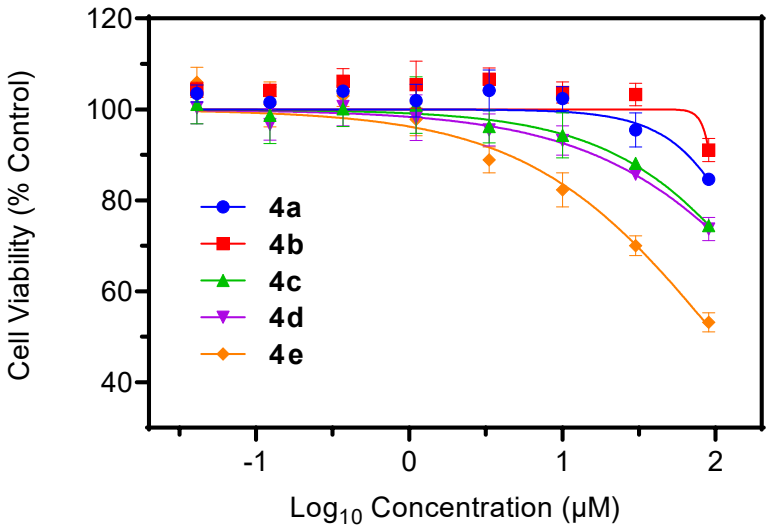

Figure 4. Cell viability assay of different quinoline *N*-oxides with HepG2 lung cancer cell. The cell viability assay was conducted 3 times for each compound at each concentration. The viability of cells without the addition of quinoline *N*-oxides was set as 100%.

Conclusions

In summary, a multifunctional hierarchical MOF catalyst was developed by the postsynthetic modification of UiO-66-NH_2, which concurrently increased the density of basic sites and created mesopores in this microporous MOF, facilitating the Knoevenagel condensation reaction. UiO-NM and PVP make Pt NPs highly dispersed on the surface of the MOF and prevents them from agglomeration, which ensures the adequate contact of substrates with active catalytic sites. MOF and PVP also synergistically enhanced the adsorption of substrates and thus the catalytic activity. The developed catalytic system was highly selective toward the formation of quinoline *N*-oxides by preventing the hydroxylamine intermediate from further hydrogenation to amine. The obtained quinoline *N*-oxides showed promising bioactivity and inhibited the proliferation of lung cancer cells in the assays. The catalyst is stable under the reaction conditions and maintans its catalytic activity after reused five times. This work represents the first to use a hierarchical MOF-metal catalyst in the tandem reaction to synthesize bioactive quinoline *N*-oxides under mild reaction conditions directly.

ASSOCIATED CONTENT

The supporting information is available free of charge on the ACS Publication websites at

Experimental details, characterization data of catalysts and products, catalytic data and recycling test of catalyst.

AUTHOR INFORMATION

Corresponding Author

*E-mail: zhiguo.zhang@zju.edu.cn

*E-mail: whuang@iastate.edu

Author Contributions

The manuscript was written through contributions of all authors. All authors have given approval to the final version of the manuscript. Z.Z. and W.H. conceived and designed the project. J.C. initialed the project, designed and conducted the experiments. B.Z., Y.P., P.H. and X.L. contributed to the preparation and general characterization of catalysts. J.C., L.Q., Z.Z. and W.H. analyzed the data and co-wrote the manuscript. R.N., Z.B., Q.Y. and Q.R. discussed the results, provided expertise and feedback. All authors have discussed the results and commented on the manuscript.

Funding Sources

We are grateful for financial support from the National Key R&D Program of China (grant number 2016YFA0202900). This work was partially supported by the National Natural Science Foundation of China (grant numbers 21878266, 21722609). W.H. appreciates the support from National Science Foundation (NSF) grant CHE-1566445. L.Q. is supported by the U.S. Department of Energy (DOE), Office of Basic Energy Sciences, Division of Chemical Sciences, Geosciences, and Biosciences. The Ames Laboratory is operated for the U.S. DOE by Iowa State University under Contract No. DE-AC02-07CH11358. J.C. thanks Zhejiang University for financial support.

Notes

The authors declare no competing financial interest.

ACKNOWLEDGMENT

We thank D. Li and co-workers for their help in testing the bioactivity of the synthesized quinoline *N*-oxides. We also thank the support from Iowa State University. We thank Gordon J. Miller for the use of the XRD instrument.

REFERENCES

(1) Nicolaou, K. C.; Edmonds, D. J.; Bulger, P. G. Cascade Reactions in Total Synthesis. *Angew. Chem., Int. Edit.* **2006,** *45*, 7134-7186.

(2) Tietze, L. F. Domino Reactions in Organic Synthesis. *Chem. Rev.* **1996,** *96*, 115-136.

(3) Gerven, T. V.; Stankiewicz, A. Structure, Energy, Synergy, Time: The Fundamentals of Process Intensification. *Ind. Eng. Chem. Res.* **2009,** *48*, 2465-2474.

(4) Wasilke, J.-C.; Obrey, S. J.; Baker, R. T.; Bazan, G. C. Concurrent Tandem Catalysis. *Chem. Rev.* **2005,** *105*, 1001-1020.

(5) Díaz, U.; Brunel, D.; Corma, A. Catalysis Using Multifunctional Organosiliceous Hybrid Materials. *Chem. Soc. Rev.* **2013,** *42*, 4083-4097.

(6) Furukawa, H.; Cordova, K. E.; O'Keeffe, M.; Yaghi, O. M. The Chemistry and Applications of Metal-Organic Frameworks. *Science* **2013,** *341*, 1230444.

(7) Dhakshinamoorthy, A.; Garcia, H. Cascade Reactions Catalyzed by Metal Organic Frameworks. *ChemSusChem* **2014,** *7*, 2392-2410.

(8) Huang, Y. B.; Liang, J.; Wang, X. S.; Cao, R. Multifunctional Metal-Organic Framework Catalysts: Synergistic Catalysis and Tandem Reactions. *Chem. Soc. Rev.* **2017,** *46*, 126-157.

(9) Liu, D.; Wan, J.; Pang, G.; Tang, Z. Hollow Metal-Organic-Framework Micro/Nanostructures and their Derivatives: Emerging Multifunctional Materials. *Adv. Mater.* **2019,** *31*, 1803291.

(10) Yuan, K.; Song, T.; Wang, D.; Zhang, X.; Gao, X.; Zou, Y.; Dong, H.; Tang, Z.; Hu, W. Effective and Selective Catalysts for Cinnamaldehyde Hydrogenation: Hydrophobic Hybrids of Metal-Organic Frameworks, Metal Nanoparticles, and Micro- and Mesoporous Polymers. *Angew. Chem., Int. Edit.* **2018,** *57*, 5708-5713.

(11) Zhao, M. T.; Yuan, K.; Wang, Y.; Li, G. D.; Guo, J.; Gu, L.; Hu, W. P.; Zhao, H. J.; Tang, Z. Y. Metal-Organic Frameworks as Selectivity Regulators for Hydrogenation Reactions. *Nature* **2016,** *539*, 76-80.

(12) Zhao, M. T.; Deng, K.; He, L. C.; Liu, Y.; Li, G. D.; Zhao, H. J.; Tang, Z. Y. Core-Shell Palladium Nanoparticle@Metal-Organic Frameworks as Multifunctional Catalysts for Cascade Reactions. *J. Am. Chem. Soc.* **2014,** *136*, 1738-1741.

(13) Deria, P.; Mondloch, J. E.; Karagiaridi, O.; Bury, W.; Hupp, J. T.; Farha, O. K. Beyond Post-Synthesis Modification: Evolution of Metal-Organic Frameworks *via* Building Block Replacement. *Chem. Soc. Rev.* **2014,** *43*, 5896-5912.

(14) Farha, O. K.; Hupp, J. T. Rational Design, Synthesis, Purification, and Activation of Metal-Organic Framework Materials. *Acc. Chem. Res.* **2010,** *43*, 1166-1175.

(15) Li, J. R.; Kuppler, R. J.; Zhou, H. C. Selective Gas Adsorption and Separation in Metal-Organic Frameworks. *Chem. Soc. Rev.* **2009,** *38*, 1477-1504.

(16) Chen, L. Y.; Luque, R.; Li, Y. W. Controllable Design of Tunable Nanostructures inside Metal-Organic Frameworks. *Chem. Soc. Rev.* **2017,** *46*, 4614-4630.

(17) Yang, Q. H.; Xu, Q.; Jiang, H. L. Metal-Organic Frameworks Meet Metal Nanoparticles: Synergistic Effect for Enhanced Catalysis. *Chem. Soc. Rev.* **2017,** *46*, 4774-4808.

(18) Lee, J.; Farha, O. K.; Roberts, J.; Scheidt, K. A.; Nguyen, S. T.; Hupp, J. T. Metal-Organic Framework Materials as Catalysts. *Chem. Soc. Rev.* **2009,** *38*, 1450-1459.

(19) Wang, Q.; Astruc, D. State of the Art and Prospects in Metal-Organic Framework (MOF)-Based and MOF-Derived Nanocatalysis. *Chem. Rev.* **2020,** *120*, 1438-1511.

(20) Guan, H.-Y.; LeBlanc, R. J.; Xie, S.-Y.; Yue, Y. Recent Progress in the Syntheses of Mesoporous Metal–Organic Framework Materials. *Coord. Chem. Rev.* **2018,** *369*, 76-90.

(21) Dhakshinamoorthy, A.; Garcia, H. Metal-Organic Frameworks as Solid Catalysts for the Synthesis of Nitrogen-Containing Heterocycles. *Chem. Soc. Rev.* **2014,** *43*, 5750-5765.

(22) Michael, J. P. Quinoline, Quinazoline and Acridone Alkaloids. *Nat. Prod. Rep.* **2008,** *25*, 166-187.

(23) Köprülü, T. K.; Ökten, S.; Tekin, Ş.; Çakmak, O. Biological Evaluation of Some Quinoline Derivatives with Different Functional Groups As Anticancer Agents. *J. Biochem. Mol. Toxic.* **2019,** *33*, e22260.

(24) Kouznetsov, V. V.; Vargas Méndez, L. Y.; Puerto Galvis, C. E.; Ortiz Villamizar, M. C. The Direct C–H Alkenylation of Quinoline N-Oxides As A Suitable Strategy for the Synthesis of Promising Antiparasitic Drugs. *New. J. Chem.* **2020,** *44*, 12-19.

(25) Scheibel, L. W.; Adler, A. Antimalarial Activity of Selected Aromatic Chelators II. Substituted Quinolines and Quinoline-*N*-Oxides. *Mol. Pharmacol.* **1981,** *20*, 218-223.

(26) de Sá, N. P.; Cisalpino, P. S.; Tavares, L. D.; Espíndola, L.; Pizzolatti, M. G.; Santos, P. C.; de Paula, T. P.; Rosa, C. A.; de Souza, D. D.; Santos, D. A.; Johann, S. Antifungal Activity of

6-Quinolinyl N-Oxide Chalcones Against Paracoccidioides. *J. Antimicrob. Chemother.* **2015,** *70*, 841-845.

(27) Malkov, A. V.; Dufková, L.; Farrugia, L.; Kočovský, P. Quinox, a Quinoline-Type *N*-Oxide, as Organocatalyst in the Asymmetric Allylation of Aromatic Aldehydes with Allyltrichlorosilanes: the Role of Arene–Arene Interactions. *Angew. Chem.* **2003,** *115*, 3802-3805.

(28) Martinez, R.; Zoli, L.; Cozzi, P. G.; Ramon, D. J.; Yus, M. Synthesis of Camphorsulfonamide-Based Quinoline Ligands and Their *N*-Oxides: First Use in the Enantioselective Addition of Organozinc Reagents to Aldehydes. *Tetrahedron: Asymmetry* **2008,** *19*, 2600-2607.

(29) Gruber, S.; Harris, C.; Kokot, E.; Lenzer, S.; Lockyer, T.; Sinn, E. Magnetic Properties and Structure of Some Copper(II) Complexes of Pyridine and Quinoline *N*-Oxides. *Aust. J. Chem.* **1967,** *20*, 2403-2413.

(30) Mautner, F. A.; Berger, C.; Fischer, R. C.; Massoud, S. S. Synthesis, Characterization and Luminescence Properties of zinc(II) and Cadmium(II) Pseudohalide Complexes Derived from Quinoline-*N*-Oxide. *Inorg. Chim. Acta* **2016,** *439*, 69-76.

(31) Wang, Y.; Zhang, L. Recent Developments in the Chemistry of Heteroaromatic *N*-Oxides. *Synthesis* **2015,** *47*, 289-305.

(32) Hwang, H.; Kim, J.; Jeong, J.; Chang, S. Regioselective Introduction of Heteroatoms at the C-8 Position of Quinoline N-Oxides: Remote C-H Activation Using N-Oxide as a Stepping Stone. *J. Am. Chem. Soc.* **2014,** *136*, 10770-10776.

(33) Yan, G.; Borah, A. J.; Yang, M. Recent Advances in Catalytic Functionalization of *N*-Oxide Compounds *via* C-H Bond Activation. *Adv. Synth. Catal.* **2014,** *356*, 2375-2394.

(34) Barsu, N.; Sen, M.; Premkumar, J. R.; Sundararaju, B. Cobalt(III) Catalyzed C-8 Selective C–H and C–O Coupling of Quinoline *N*-Oxide with Internal Alkynes *via* C–H Activation and Oxygen Atom Transfer. *Chem. Commun.* **2016,** *52*, 1338-1341.

(35) Kim, J.; Kim, S.; Kim, D.; Chang, S. Ru-Catalyzed Deoxygenative Regioselective C8-H Arylation of Quinoline N-Oxides. *J. Org. Chem.* **2019,** *84*, 13150-13158.

(36) Dhiman, A. K.; Gupta, S. S.; Sharma, R.; Kumar, R.; Sharma, U. Rh(III)-Catalyzed C(8)–H Activation of Quinoline N-Oxides: Regioselective C–Br and C–N Bond Formation. *J. Org. Chem.* **2019,** *84*, 12871-12880.

(37) Dyer, R. M. B.; Hahn, P. L.; Hilinski, M. K. Selective Heteroaryl N-Oxidation Of Amine-Containing Molecules. *Org. Lett.* **2018,** *20*, 2011-2014.

(38) Palav, A.; Misal, B.; Ernolla, A.; Parab, V.; Waske, P.; Khandekar, D.; Chaudhary, V.; Chaturbhuj, G. The m-CPBA–NH_3(g) System: A Safe and Scalable Alternative for the Manufacture of (Substituted) Pyridine and Quinoline N-Oxides. *Org. Process Res. Dev.* **2019,** *23*, 244-251.

(39) Basu, P.; Prakash, P.; Gravel, E.; Shah, N.; Bera, K.; Doris, E.; Namboothiri, I. N. N. Carbon Nanotube–Ruthenium Hybrids for the Partial Reduction of 2-Nitrochalcones: Easy Access to Quinoline *N*-Oxides. *ChemCatChem* **2016,** *8*, 1298-1302.

(40) Lee, K. Y.; Kim, J. M.; Kim, J. N. Synthesis of 3-Substituted-4-Hydroxyquinoline *N*-Oxides from the Baylis-Hillman Adducts of *o*-Nitrobenzaldehydes. *Tetrahedron* **2003,** *59*, 385-390.

(41) Liu, Y.; Wang, C.; Lv, N. N.; Liu, Z. X.; Zhang, Y. H. Synthesis of Quinoline *N*-Oxides by Cobalt-Catalyzed Annulation of Arylnitrones And Alkynes. *Adv. Synth. Catal.* **2017,** *359*, 1351-1358.

(42) Colacino, E.; Andre, C.; Martinez, J.; Lamaty, F. Synthesis of a Novel Pyrrolo-[3,2-c]Quinoline *N*-oxide by aza-Baylis-Hillman Adduct of *o*-Nitrobenzaldehyde. *Tetrahedron Lett.* **2008,** *49*, 4953-4955.

(43) Bujok, R.; Wrobel, Z.; Wojciechowski, K. Simple Synthesis of 4-Cyanoquinoline *N*-Oxides. *Tetrahedron Lett.* **2016,** *57*, 1014-1018.

(44) Familoni, O. B.; Klaas, P. J.; Lobb, K. A.; Pakade, V. E.; Kaye, P. T. The Baylis‐Hillman Approach to Quinoline Derivatives. *Org. Biomol. Chem.* **2006,** *4*, 3960-3965.

(45) Zhu, L.; Liu, X. Q.; Jiang, H. L.; Sun, L. B. Metal-Organic Frameworks for Heterogeneous Basic Catalysis. *Chem. Rev.* **2017,** *117*, 8129-8176.

(46) Chen, J.; Liu, R.; Gao, H.; Chen, L.; Ye, D. Amine-Functionalized Metal-Organic Frameworks for the Transesterification of Triglycerides. *J. Mater. Chem. A* **2014,** *2*, 7205-7213.

(47) Schaate, A.; Roy, P.; Godt, A.; Lippke, J.; Waltz, F.; Wiebcke, M.; Behrens, P. Modulated Synthesis of Zr-Based Metal-Organic Frameworks: from Nano to Single Crystals. *Chem.—Eur. J.* **2011,** *17*, 6643-6651.

(48) Katz, M. J.; Brown, Z. J.; Colon, Y. J.; Siu, P. W.; Scheidt, K. A.; Snurr, R. Q.; Hupp, J. T.; Farha, O. K. A Facile Synthesis of UiO-66, UiO-67 and Their Derivatives. *Chem. Commun.* **2013,** *49*, 9449-9451.

(49) Trickett, C. A.; Gagnon, K. J.; Lee, S.; Gandara, F.; Buergi, H.-B.; Yaghi, O. M. Definitive Molecular Level Characterization of Defects in UiO-66 Crystals. *Angew. Chem., Int. Edit.* **2015,** *54*, 11162-11167.

(50) Yang, P.; Mao, F.; Li, Y.; Zhuang, Q.; Gu, J. Hierarchical Porous Zr-Based MOFs Synthesized by a Facile Monocarboxylic Acid Etching Strategy. *Chem.—Eur. J.* **2018,** *24*, 2962-2970.

(51) Wei, J.; Cheng, N.; Liang, Z.; Wu, Y.; Zou, Z.; Zhuang, Z.; Yu, Y. Heterometallic Metal-Organic Framework Nanocages of High Crystallinity: An Elongated Channel Structure Formed In Situ through Metal-Ion (M = W or Mo) Doping. *J. Mater. Chem. A* **2018,** *6*, 23336-23344.

(52) Zhao, Y.; Zhang, Q.; Li, Y.; Zhang, R.; Lu, G. Large-Scale Synthesis of Monodisperse UiO-66 Crystals with Tunable Sizes and Missing Linker Defects via Acid/Base Co-Modulation. *ACS Appl. Mater. Interfaces* **2017,** *9*, 15079-15085.

(53) Guo, Z. Y.; Xiao, C. X.; Maligal-Ganesh, R. V.; Zhou, L.; Goh, T. W.; Li, X. L.; Tesfagaber, D.; Thiel, A.; Huang, W. Y. Pt Nanoclusters Confined within Metal Organic Framework Cavities for Chemoselective Cinnamaldehyde Hydrogenation. *ACS Catal.* **2014,** *4*, 1340-1348.

(54) Duan, P.; Moreton, J. C.; Tavares, S. R.; Semino, R.; Maurin, G.; Cohen, S. M.; Schmidt-Rohr, K. Polymer Infiltration into Metal–Organic Frameworks in Mixed-Matrix Membranes Detected In Situ by NMR. *J. Am. Chem. Soc.* **2019,** *141*, 7589-7595.

(55) Ding, M.; Jiang, H.-L. Incorporation of Imidazolium-Based Poly(Ionic Liquid)s into a Metal–Organic Framework for CO_2 Capture and Conversion. *ACS Catal.* **2018,** *8*, 3194-3201.

(56) Cirujano, F. G.; Leyva-Pérez, A.; Corma, A.; Llabrés i Xamena, F. X. MOFs as Multifunctional Catalysts: Synthesis of Secondary Arylamines, Quinolines, Pyrroles, and Arylpyrrolidines over Bifunctional MIL-101. *ChemCatChem* **2013,** *5*, 538-549.

(57) Okuma, K.; Seto, J.; Nagahora, N.; Shioji, K. Chemoselective Synthesis of Quinoline *N*-Oxides from 3-(2-Nitrophenyl)-3-Hydroxypropanones. *J. Heterocyclic Chem.* **2010,** *47*, 1372-1378.

Table of Contents